JOURNAL OF GUIDANCE, CONTROL, AND DYNAMICS
Vol. 30, No. 4, July–August 2007

Engineering Notes

ENGINEERING NOTES are short manuscripts describing new developments or important results of a preliminary nature. These Notes should not exceed 2500 words (where a figure or table counts as 200 words). Following informal review by the Editors, they may be published within a few months of the date of receipt. Style requirements are the same as for regular contributions (see inside back cover).

Launch Vehicle Autopilot Robustness to Multilinear Uncertainties: Analysis in Kharitonov Framework

V. R. Lalithambika*
Vikram Sarabhai Space Center, Trivandrum, Kerala 695 022, India
and
S. Dasgupta†
Mohandas College of Engineering and Technology, Trivandrum, Kerala 695 544, India

DOI: 10.2514/1.27766

I. Introduction

THE launch vehicle plant is time varying in nature and the system parameters such as center of gravity, moment of inertia, thrust, aerodynamics, and structural parameters such as mode shape, stiffness, and generalized mass vary continuously from ignition to burnout, with definite uncertainty bounds for each parameter. For an aerodynamically unstable launch vehicle in the atmospheric flight regime, the low frequency gain margin associated with the aerodynamic instability is as important as the rigid body gain and phase margins, and the lag and lead phase margins for the phase stabilized dominant flexible mode [1]. Hence, a launch vehicle control system has multiple gain and phase margins to be considered, corresponding to the unstable aerodynamics, rigid body, and the bending mode.

The flexibility of the vehicle enters the control problem because the attitude sensors (gyros) pick up the local elastic distortions in addition to the rigid body motion. Because the rate gyro location is close to the antinode (zero slope point) of the first bending mode shape, uncertainty in the mode shape causes large change in the mode slope at the rate gyro location, which can even change sign from positive to negative. This in turn leads to large amplitude and phase swing for the phase stabilized bending mode.

The system has a large number of uncertain parameters consisting of the vehicle rigid body, flexible mode, and aerodynamic parameters. The system also has a multilinear uncertainty structure, i.e., when all the uncertain parameters except one are held constant, the coefficients of the system transfer function are linear functions of the variable parameter. The robustness analysis of such systems requires the evaluation of the entire family of systems and is usually carried out by one of two methods; the first is to evaluate all possible combinations of parameter perturbations with the candidate controller in loop. This approach of gridding the uncertain set is extremely cumbersome for complex systems. The second method is to choose appropriate combinations of parameter perturbations to generate worst case bounds and evaluate this set of systems. Because the choice of the combination of perturbed parameters is left to the designer's judgment, there is a possibility of missing the worst case due to the large number of uncertain parameters.

This Note offers an alternative, systematic approach to robust stability analysis of this challenging real-life system with multilinear uncertainty structure and with multiple minimum phase margin and gain margin points, based on the Kharitonov theorem and the mapping theorem [2]. The generalized Kharitonov theorem is used to generate bounds on the system transfer functions. The mapping theorem is used to get the boundary of the image sets of the entire family, through the image set of the extremal sets. The robustness of the system is evaluated through frequency response analysis. The uncertain plant set is also generated through gridding and the stability margins so obtained compared with those of the Kharitonov approach.

The Kharitonov theorem is an extension of the Routh stability criterion to polynomials with real parametric independent uncertainty structure [3]. Chapellat and Bhattacharyya have generalized the Kharitonov theorem to cater to affine linear and multilinear uncertain systems [4]. The generalized Kharitonov theorem gives necessary and sufficient conditions for stabilization of an interval plant. Chapellat and Dahleh [5] present a complete set of results concerning the robust stability analysis of single-input/single-output interval plants and introduce the Kharitonov segments associated with an interval plant. A comprehensive survey of extreme point results for systems with structured real parametric uncertainty, covering both robust stability and robust performance is given in [6]. Hollot and Tempo [7] show that for a robustly stable interval feedback system, large and critical portions of the Nyquist envelope, including the minimum gain margin and minimum phase margin points, are covered by the Kharitonov plants. This result extends the use of the Nyquist plots to the domain of control systems containing parameter uncertainty. The conditions given by Hollot and Tempo for the minimum gain margin and minimum phase margin points in the Nyquist envelope to be covered by the Kharitonov plants are satisfied for the launch vehicle system with multiple minimum gain and phase margins also. This result is used in this Note for robust stability analysis.

II. System Model

For design and analysis, a time-slice approach is used, with the vehicle parameters assumed frozen for a short time duration. The plant model consists of a rigid body, aerodynamics, flexibility, and actuator dynamics. A proportional derivative PD controller that provides adequate stability margins for the nominal system (the design plant) with phase stabilization of the bending mode is chosen as the candidate controller for system robustness evaluation. A typical aerodynamically unstable, flexible launch vehicle during atmospheric flight is shown in Fig. 1.

Here, X_b and Z_b are the body axes in the pitch plane, l is the length parameter along the vehicle longitudinal axis, θ is the perturbation attitude angle, α the angle of attack, l_α the aerodynamic moment arm length, S the reference surface area, Q the dynamic pressure, V_R the

Received 16 September 2006; revision received 21 December 2006; accepted for publication 27 December 2006.

*Head, Mission Simulation and Analysis Division, Control, Guidance, and Simulation Entity, Vikram Sarabhai Space Center, Trivandrum, Kerala, India.

†Head of Department of Electrical Engineering, Mohandas College of Engineering and Technology, Trivandrum, Kerala, India.

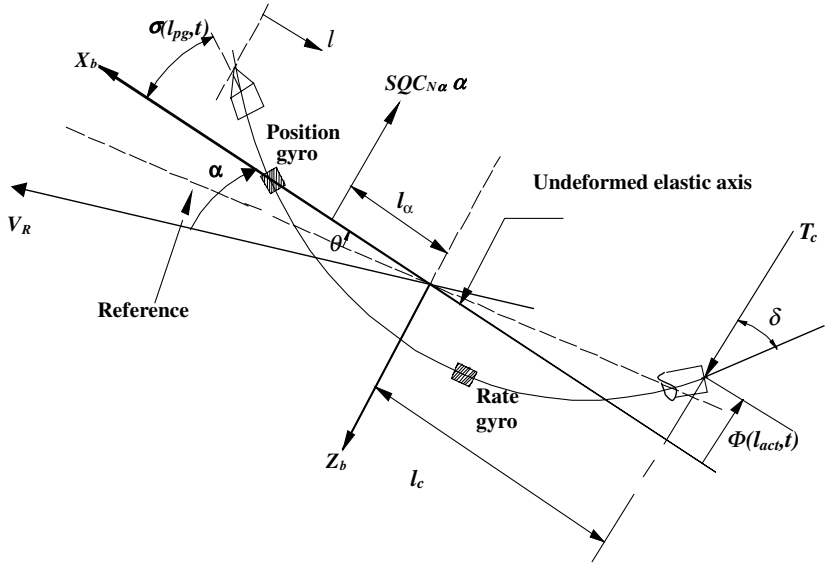

Fig. 1 Elastic vehicle in the pitch plane.

relative velocity vector, and $C_{N\alpha}$ the aerodynamic normal force coefficient. The bending mode slope at position gyro location is $\sigma(l_{\text{pg}}, t)$; $\phi(l_{\text{act}}, t)$ is the bending mode deflection at the actuator location, T_c the control force, l_c the control moment arm, and δ the engine deflection angle.

The short period equations of motion are as follows:

Moment equation

$$I_{yy}\ddot{\theta} = L_\alpha l_a \theta + T_c l_c(\delta_a - \sigma_{l_{\text{act}}} q) \tag{1}$$

where

$$L_\alpha = SQC_{N\alpha}$$

Flexibility equation

$$M\ddot{q} = -T_c \phi_{l_{\text{act}}}(\delta_a - \sigma_{l_{\text{act}}} q) - Kq - B\dot{q} \tag{2}$$

Actuator dynamics

$$\ddot{\delta}_a = \omega_a^2 \delta_c - 2\zeta_a \omega_a \dot{\delta}_a - \omega_a^2 \delta_a \tag{3}$$

Sensed attitude angle

$$\theta_s = \theta + \sigma_{l_{\text{pg}}} q \tag{4}$$

Sensed body rate

$$\dot{\theta}_s = \dot{\theta} + \sigma_{l_{\text{rg}}} \dot{q} \tag{5}$$

Here, q is the normalized coordinate of bending, δ_c is the command to actuator, ω_a is the actuator bandwidth, ζ_a is the actuator damping factor, δ_a is the actuator deflection angle, I_{yy} is the moment of inertia about pitch axis, and M, K, and B are the generalized mass, stiffness, and damping coefficient, respectively, of the bending mode. The bending mode slopes at position gyro, rate gyro, and actuator locations are $\sigma_{l\text{pg}}$, $\sigma_{l\text{rg}}$, and $\sigma_{l\text{act}}$, respectively, and $\phi_{l\text{act}}$ is the bending deflection at actuator location. The effect of the bending mode slope at the actuator location $\sigma_{l\text{act}} q$ on the system response is generally small and this quantity has been neglected to simplify the analysis. The model parameter values are given in Table 1 along with the controller parameters K_A and K_R.

The plant with controller is shown in Fig. 2. The open loop transfer function for the system is

$$L(s) = \frac{K_A \omega_a^2 T_c l_c (K_R s + 1)(Ms^2 + Bs + K) - K_A \omega_a^2 T_c \phi_{l_{\text{act}}}(I_{yy} s^2 - L_\alpha l_\alpha)(\sigma_{l_{\text{pg}}} + \sigma_{l_{\text{rg}}} K_R s)}{(I_{yy} s^2 - L_\alpha l_\alpha)(s^2 + 2\zeta_a \omega_a s + \omega_a^2)(Ms^2 + Bs + K)} \tag{6}$$

Table 1 Nominal and off-nominal model parameter values

Fixed parameters		Variable parameters			
Quantity	Value	Quantity	Nominal	Lower bound	Upper bound
ω_a	18.9 rad/s	L_α	4,515,808 N/rad	4,064,227 N/rad	4,967,389 N/rad
ζ_a	0.7	l_α	1.78 m	0.778 m	2.778 m
T_c	1,377,180 N	M	2804 kg	2524 kg	3084 kg
l_c	11.91 m	K	395,002 N/m	355,502 N/m	434,502 N/m
I_{yy}	23,495,230 kg m^2	B	665.6	599	732.2
K_A	8.16	$\sigma_{l\text{pg}}$	0.062	0.058	0.071
K_R	0.9	$\sigma_{l\text{rg}}$	−0.27E-03	−0.009	0.0037
——	——	$\sigma_{l\text{act}}$	0.091	0.082	0.101

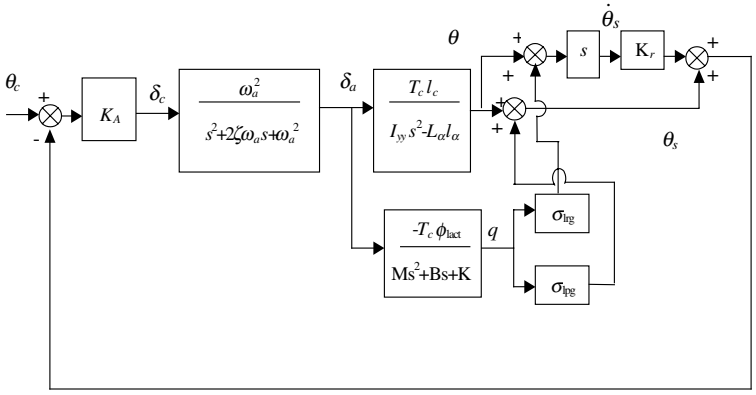

Fig. 2 System model.

With parametric uncertainties on the bending mode and aerodynamic parameters, Eq. (6) can be rewritten as

$$L(s) = \frac{(C_1 s + C_2)P_1 - P_2 P_3 P_4}{(s^2 + C_3 s + C_4)P_1 P_3} \tag{7}$$

where $C_1, \ldots, C_4$ are constants described by $C_1 = K_A \omega_a^2 T_c l_c K_R$, $C_2 = K_A \omega_a^2 T_c l_c$, $C_3 = 2\zeta_a \omega_a$, and $C_4 = \omega_a^2$; and $P_1, \ldots, P_4$ are uncertain polynomials described by $P_1 = (Ms^2 + Bs + K)$, $P_2 = K_A \omega_a^2 T_c \phi_{l_{\text{act}}}$, $P_3 = (I_{yy}s^2 - L_\alpha l_\alpha)$, and $P_4 = (\sigma_{l_{\text{pg}}} + \sigma_{l_{\text{rg}}} K_R s)$.

The system has a multilinear uncertainty structure with common terms in numerator and denominator and uncertainties in the bending mode parameters M, B, K, σ_{pg}, σ_{rg}, and ϕ, and aerodynamic parameters L_α and l_α.

III. Robust Stability Analysis

Four Kharitonov polynomials are associated with each uncertain polynomial $A(s) = a_0 + a_1 s + \cdots + a_n s^n$. If the first Kharitonov polynomial is denoted by $K_1(s) = a_0^u + a_1^u s + a_2^l s^2 + a_3^l s^3 + a_4^u s^4 + \cdots$ with the repetitive sequence of uncertain parameter combinations $uull\ldots$, the other three polynomials have the combinations $ullu\ldots$, $luul\ldots$, and $lluu\ldots$, respectively, where subscript l denotes the lower bound and subscript u denotes the upper bound of each parameter. Using the generalized Kharitonov theorem, each of the uncertain polynomials is replaced by the corresponding extremal polynomial manifolds, constructed by joining appropriate pairs of Kharitonov polynomials. The extremal set of transfer functions is then formed and the image set of the extremal systems at $s = j\omega$ evaluated. By the mapping theorem, the complex plane image set of the entire family of systems at $s = j\omega$ is concave, or bulges inward, and hence is overbounded by the image set of the extremal systems. The analysis of the image set of the extremal systems gives the guaranteed gain and phase margins of the entire family.

The Kharitonov polynomials and segments associated with the uncertain polynomials of the system in Eq. (7) are constructed through straightforward calculations and the extremal multilinear interval family is obtained, as follows:

The four Kharitonov polynomials associated with P_1 are

$$\begin{aligned} K_{11} &= (M^l s^2 + B^u s + K^u), \qquad K_{12} = (M^l s^2 + B^l s + K^u) \\ K_{13} &= (M^u s^2 + B^u s + K^l), \qquad K_{14} = (M^u s^2 + B^l s + K^l) \end{aligned} \tag{8}$$

The two Kharitonov polynomials of P_2 are

$$K_{21} = K_A \omega_a^2 T_c \phi_{l\text{act}}^u, \qquad K_{22} = K_A \omega_a^2 T_c \phi_{l\text{act}}^l \tag{9}$$

and those of P_3 are

$$K_{31} = (I_{yy}s^2 - L_\alpha^l l_\alpha^l), \qquad K_{32} = (I_{yy}s^2 - L_\alpha^u l_\alpha^u) \tag{10}$$

The four Kharitonov polynomials of P_4 are

$$\begin{aligned} K_{41} &= (\sigma_{l_{\text{pg}}}^u + \sigma_{l_{\text{rg}}}^u K_R s), \qquad K_{42} = (\sigma_{l_{\text{pg}}}^l + \sigma_{l_{\text{rg}}}^u K_R s) \\ K_{43} &= (\sigma_{l_{\text{pg}}}^u + \sigma_{l_{\text{rg}}}^l K_R s), \qquad K_{44} = (\sigma_{l_{\text{pg}}}^l + \sigma_{l_{\text{rg}}}^l K_R s) \end{aligned} \tag{11}$$

The extremal multilinear interval family is constructed as

$$S1 = \frac{(C_1 s + C_2)K_{1i} - K_{2j}K_{3k}[\lambda K_{41} + (1-\lambda)K_{42}]}{(s^2 + C_3 s + C_4)K_{1i}K_{3k}} \tag{12}$$

$$S2 = \frac{(C_1 s + C_2)K_{1i} - K_{2j}K_{3k}[\lambda K_{41} + (1-\lambda)K_{43}]}{(s^2 + C_3 s + C_4)K_{1i}K_{3k}} \tag{13}$$

$$S3 = \frac{(C_1 s + C_2)K_{1i} - K_{2j}K_{3k}[\lambda K_{42} + (1-\lambda)K_{44}]}{(s^2 + C_3 s + C_4)K_{1i}K_{3k}} \tag{14}$$

$$S4 = \frac{(C_1 s + C_2)K_{1i} - K_{2j}K_{3k}[\lambda K_{43} + (1-\lambda)K_{44}]}{(s^2 + C_3 s + C_4)K_{1i}K_{3k}} \tag{15}$$

$$S5 = \frac{(C_1 s + C_2)K_{1i} - K_{2j}K_{4l}[\lambda K_{31} + (1-\lambda)K_{32}]}{(s^2 + C_3 s + C_4)K_{1i}[\lambda K_{31} + (1-\lambda)K_{32}]} \tag{16}$$

$$S6 = \frac{(C_1 s + C_2)K_{1i} - [\lambda K_{21} + (1-\lambda)K_{22}]K_{3k}K_{4l}}{(s^2 + C_3 s + C_4)K_{1i}K_{3k}} \tag{17}$$

$$S7 = \frac{(C_1 s + C_2)[\lambda K_{11} + (1-\lambda)K_{12}] - K_{2j}K_{3k}K_{4l}}{(s^2 + C_3 s + C_4)[\lambda K_{11} + (1-\lambda)K_{12}]K_{3k}} \tag{18}$$

$$S8 = \frac{(C_1 s + C_2)[\lambda K_{11} + (1-\lambda)K_{13}] - K_{2j}K_{3k}K_{4l}}{(s^2 + C_3 s + C_4)[\lambda K_{11} + (1-\lambda)K_{13}]K_{3k}} \tag{19}$$

$$S9 = \frac{(C_1 s + C_2)[\lambda K_{12} + (1-\lambda)K_{14}] - K_{2j}K_{3k}K_{4l}}{(s^2 + C_3 s + C_4)[\lambda K_{12} + (1-\lambda)K_{14}]K_{3k}} \tag{20}$$

$$S10 = \frac{(C_1 s + C_2)[\lambda K_{13} + (1-\lambda)K_{14}] - K_{2j}K_{3k}K_{4l}}{(s^2 + C_3 s + C_4)[\lambda K_{13} + (1-\lambda)K_{14}]K_{3k}} \tag{21}$$

for $i = 1{:}4$, $j = 1{:}2$, $k = 1{:}2$, and $l = 1{:}4$, with $\lambda = \begin{bmatrix} 0 & 1 \end{bmatrix}$.

The mapping theorem is used to get the boundary of the image sets of the entire family, through the image set of the extremal sets at

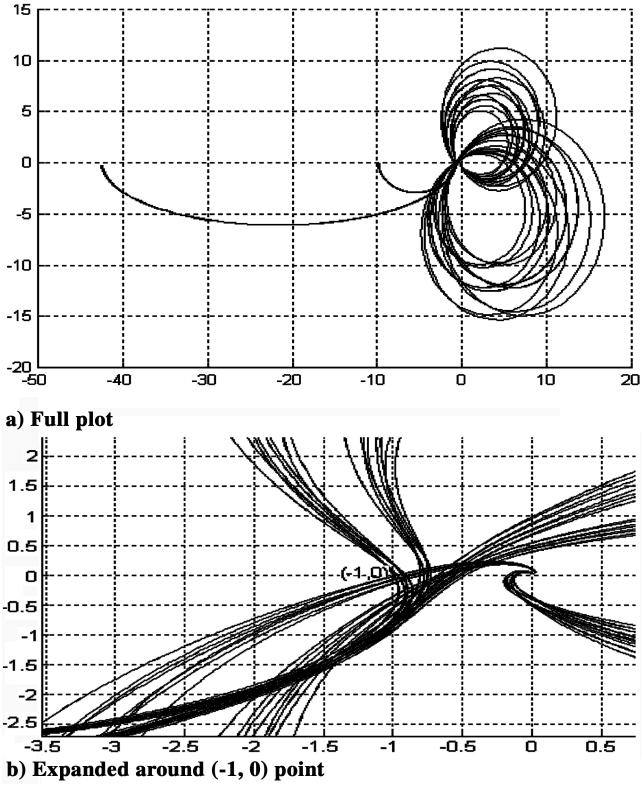

Fig. 3 Nyquist plot of extremal systems.

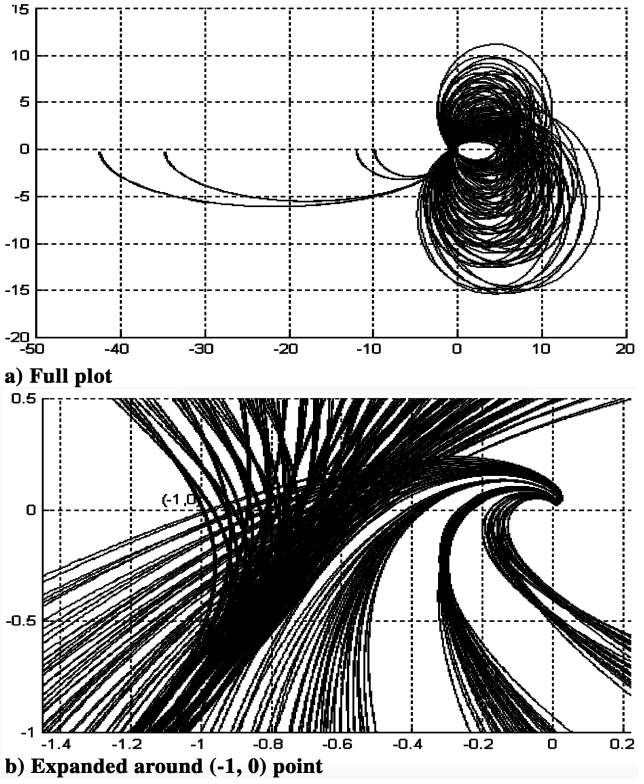

Fig. 4 Nyquist plot of systems with gridding.

$s = j\omega$. The frequency range chosen is from 0 to 8 Hz, because the highest system dynamic frequency is 4 Hz. The Nyquist plots of the image sets of the extremal systems are given in Fig. 3a with the region around $(-1, 0)$ point expanded in Fig. 3b. The minimum gain and phase margins corresponding to the rigid body, and the phase lag and phase lead margins for the bending mode, are obtained from the Nyquist plots. The response plots show large swing in the phase of the system flexible mode over the extremal set. This is due to the large uncertainty in the bending mode slope at the rate gyro location. With the designed classical controller, the low-frequency gain margin (aeromargin, corresponding to aerodynamic uncertainties) was seen to be 20 dB and the minimum rigid body phase margin was seen to be more than 8 deg. Because the worst case stability margins obtained for the image set of the extremal systems are the guaranteed stability margins for the entire set, these margins are adequate. However, the rigid body gain margin is seen to be significantly affected by the swing in the bending mode phase, due to the proximity of the first bending mode frequency to the gain margin frequency. The bending mode lag and lead phase margins are also very low and the system is marginally stable at the bending mode frequency for some of the extremal systems. Hence, the current controller is just sufficient to robustly stabilize the system.

Because the image set of the extremal systems overbounds the image set of the entire family, some conservatism is expected in the results. To assess the degree of conservatism, a set of systems have been formed with the brute force approach of gridding, i.e., varying each uncertain parameter over its allowable range with the other parameters held constant (Fig. 4). The extremal system frequency responses were compared with the system response with gridding. It was seen that the extremal systems capture the minimum phase margin, gain margin, aeromargin, the lag and lead margins for the bending mode, as well as the peak mode magnitude with very little conservatism. The guaranteed margins for all the dynamics are thus obtained by analyzing the extremal set.

IV. Conclusions

The extremal multilinear interval family associated with the aerodynamically unstable, flexible launch vehicle control system is constructed and the minimum rigid body and flexible mode phase and gain margins are obtained by frequency response analysis. The conservatism of the results is assessed by comparison with results obtained by gridding the uncertain set. It is shown that the Kharitonov approach gives a realistic assessment of the robust stability of the system with very little conservatism. The feasibility of this approach for real-life problems with multilinear uncertainty structure and multiple minimum gain and phase margins is demonstrated.

References

[1] Greensite, A. L., *Analysis and Design of Space Vehicle Flight Control Systems*, Control Theory, Vol. 2, Spartan, New York, 1970, pp. 15–283.

[2] Bhattacharyya, S. P., Chapellat, H., and Keel, L. H., *Robust Control: the Parametric Approach*, Prentice Hall Information and System Sciences Series, Prentice–Hall, Upper Saddle River, NJ, 1995, pp. 293–484.

[3] Kharitonov, V. L., "Asymptotic Stability of an Equilibrium Position of a Family of Systems of Linear Differential Equations," *Differential Equations*, Vol. 14, 1979, pp. 1483–1485.

[4] Chapellat, H., and Bhattacharyya, S. P., "Generalization of Kharitonov's Theorem: Robust Stability of Interval Plants," *IEEE Transactions on Automatic Control*, Vol. 34, No. 3, 1989, pp. 306–311.

[5] Chapellat, H., and Dahleh, M., "Robust Stability of Interval Plants: a Review," *Proceedings of the American Control Conference*, Vol. 3, IEEE Publications/American Automatic Control Council,, Piscataway, NJ, July 1990, pp. 2548–2553.

[6] Barmish, B. R., and Kang, H. I., "Survey of Extreme Point Results for Robustness of Control Systems," *Automatica*, Vol. 29, No. 1, 1993, pp. 13–35.

[7] Hollot, C. V., and Tempo, R., "Nyquist Envelope of an Interval Plant Family," *IEEE Transactions on Automatic Control*, Vol. 39, No. 2, 1994, pp. 391–396.